Effect of nonstationarities on detrended fluctuation analysis

Zhi Chen,[1] Plamen Ch. Ivanov,[1,2] Kun Hu,[1] H. Eugene Stanley[1]

[1]*Center for Polymer Studies and Department of Physics, Boston University, Boston, Massachusetts 02215*
[2]*Harvard Medical School, Beth Israel Deaconess Medical Center, Boston, Massachusetts 02215*
(Received 12 November 2001; published 8 April 2002)

Detrended fluctuation analysis (DFA) is a scaling analysis method used to quantify long-range power-law correlations in signals. Many physical and biological signals are "noisy," heterogeneous, and exhibit different types of nonstationarities, which can affect the correlation properties of these signals. We systematically study the effects of three types of nonstationarities often encountered in real data. Specifically, we consider nonstationary sequences formed in three ways: (i) stitching together segments of data obtained from discontinuous experimental recordings, or removing some noisy and unreliable parts from continuous recordings and stitching together the remaining parts—a "cutting" procedure commonly used in preparing data prior to signal analysis; (ii) adding to a signal with known correlations a tunable concentration of random outliers or spikes with different amplitudes; and (iii) generating a signal comprised of segments with different properties—e.g., different standard deviations or different correlation exponents. We compare the difference between the scaling results obtained for stationary correlated signals and correlated signals with these three types of nonstationarities. We find that introducing nonstationarities to stationary correlated signals leads to the appearance of crossovers in the scaling behavior and we study how the characteristics of these crossovers depend on (a) the fraction and size of the parts cut out from the signal, (b) the concentration of spikes and their amplitudes (c) the proportion between segments with different standard deviations or different correlations and (d) the correlation properties of the stationary signal. We show how to develop strategies for preprocessing "raw" data prior to analysis, which will minimize the effects of nonstationarities on the scaling properties of the data, and how to interpret the results of DFA for complex signals with different local characteristics.

PACS number(s): 05.40.−a

I. INTRODUCTION

In recent years, there has been growing evidence indicating that many physical and biological systems have no characteristic length scale and exhibit long-range power-law correlations. Traditional approaches such as the power-spectrum and correlation analysis are suited to quantify correlations in stationary signals [1,2]. However, many signals that are outputs of complex physical and biological systems are nonstationary—the mean, standard deviation, and higher moments, or the correlation functions are not invariant under time translation [1,2]. Nonstationarity, an important aspect of complex variability, can often be associated with different trends in the signal or heterogeneous segments (patches) with different local statistical properties. To address this problem, detrended fluctuation analysis (DFA) was developed to accurately quantify long-range power-law correlations embedded in a nonstationary time series [3,4]. This method provides a single quantitative parameter—the scaling exponent α—to quantify the correlation properties of a signal. One advantage of the DFA method is that it allows the detection of long-range power-law correlations in noisy signals with embedded polynomial trends that can mask the true correlations in the fluctuations of a signal. The DFA method has been successfully applied to research fields such as DNA [3,5–16], cardiac dynamics [17–37], human gait [38], meteorology [39], climate temperature fluctuations [40–42], river flow and discharge [43,44], neural receptors in biological systems [45], and economics [46–58]. The DFA method may also help identify different states of the same system with different scaling behavior—e.g., the scaling exponent α

for heartbeat intervals is different for healthy and sick individuals [17,28] as well as for waking and sleeping states [23,33].

To understand the intrinsic dynamics of a given system, it is important to analyze and correctly interpret its output signals. One of the common challenges is that the scaling exponent is not always constant (independent of scale) and crossovers often exist—i.e., the value of the scaling exponent α differs for different ranges of scales [17,18,23,59,60]. A crossover is usually due to a change in the correlation properties of the signal at different time or space scales, though it can also be a result of nonstationarities in the signal. A recent work considered different types of nonstationarities associated with different trends (e.g., polynomial, sinusoidal, and power-law trends) and systematically studied their effect on the scaling behavior of long-range correlated signals [61]. Here we consider the effects of three other types of nonstationarities, which are often encountered in real data or result from "standard" data preprocessing approaches.

(a) Signals with segments removed. First we consider a type of nonstationarity caused by discontinuities in signals. Discontinuities may arise from the nature of experimental recordings, e.g., stock exchange data are not recorded during the nights, weekends, and holidays [46–53]. Alternatively, discontinuities may be caused by the fact that some noisy and unreliable portions of continuous recordings must be discarded, as often occurs when analyzing physiological signals [17–37]. In this case, a common preprocessing procedure is to cut out the noisy, unreliable parts of the recording and stitch together the remaining informative segments before any statistical analysis is performed. One immediate problem

is how such cutting procedure will affect the scaling properties of long-range correlated signals. A careful consideration should be made when interpreting results obtained from scaling analysis, so that an accurate estimate of the true correlation properties of the original signal may be obtained.

(b) Signals with random spikes. A second type of nonstationarity is due to the existence of spikes in data, which is very common in real life signals [17–38]. Spikes may arise from external conditions that have little to do with the intrinsic dynamics of the system. In this case, we must distinguish the spikes from normal intrinsic fluctuations in the system's output and filter them out when we attempt to quantify correlations. Alternatively, spikes may arise from the intrinsic dynamics of the system, rather than being an epiphenomenon of external conditions. In this second case, careful considerations should be made as to whether the spikes should be filtered out when estimating correlations in the signal, since such "intrinsic" spikes may be related to the properties of the noisy fluctuations. Here, we consider only the simpler case, namely, when the spikes are independent of the fluctuations in the signal. The problem is how spikes affect the scaling behavior of correlated signals, e.g., what kind of crossovers they may possibly cause. We also demonstrate to what extent features of the crossovers depend on the statistical properties of the spikes. Furthermore, we show how to recognize if a crossover indeed indicates a transition from one type of underlying correlations to a different type, or if the crossover is due to spikes without any transition in the dynamical properties of the fluctuations.

(c) Signals with different local behavior. A third type of nonstationarity is associated with the presence of segments in a signal that exhibit different local statistical properties, e.g., different local standard deviations or different local correlations. Some examples include the following: (a) 24-h records of heart rate fluctuations are characterized by segments with larger standard deviation during stress and physical activity and segments with smaller standard deviation during rest [19]; (b) studies of DNA show that coding and noncoding regions are characterized by different types of correlations [5,8]; (c) brain wave analysis of different sleep stages (rapid eye movement sleep, light sleep, and deep sleep) indicates that the signal during each stage may have different correlation properties [62]; (d) heartbeat signals during different sleep stages exhibit different scaling properties [33]. For such complex signals, results from scaling analysis often reveal a very complicated structure. It is a challenge to quantify the correlation properties of these signals. Here, we take a first step toward understanding the scaling behavior of such signals.

We study these three types of nonstationarities embedded in correlated signals. We apply the DFA method to stationary correlated signals and identical signals with artificially imposed nonstationarities, and compare the difference in the scaling results. (i) We find that cutting segments from a signal and stitching together the remaining parts does not affect the scaling for positively correlated signals. However, this cutting procedure strongly affects anticorrelated signals, leading to a crossover from an anticorrelated regime (at small scales) to an uncorrelated regime (at large scales). (ii)

For the correlated signals with superposed random spikes, we find that the scaling behavior is a superposition of the scaling of the signal and the apparent scaling of the spikes. We analytically prove this superposition relation by introducing a *superposition rule*. (iii) For the case of complex signals comprised of segments with different local properties, we find that their scaling behavior is a superposition of the scaling of the different components—each component containing only the segments exhibiting identical statistical properties. Thus, to obtain the scaling properties of the signal, we need only to examine the properties of each component—a much simpler task than analyzing the original signal.

The layout of the paper is as follows: In Sec. II, we describe how we generate signals with desired long-range correlation properties and introduce the DFA method to quantify these correlations. In Sec. III, we compare the scaling properties of correlated signals before and after removing some segments from the signals. In Sec. IV, we consider the effect of random spikes on correlated signals. We show that the superposition of spikes and signals can be explained by a superposition rule derived in Appendix A. In Sec. V, we study signals comprised of segments with different local behavior. We systematically examine all resulting crossovers, their conditions of existence, and their typical characteristics associated with the different types of nonstationarities. We summarize our findings in Sec. VI.

II. METHOD

Using a modified Fourier filtering method [63], we generate stationary uncorrelated, correlated, and anticorrelated signals $u(i)$ ($i=1,2,3,\ldots,N_{max}$) with a standard deviation $\sigma=1$. This method consists of the following steps.

(a) First, we generate an uncorrelated and Gaussian distributed sequence $\eta(i)$ and calculate the Fourier transform coefficients $\eta(q)$.

(b) The desired signal $u(i)$ must exhibit correlations that are defined by the form of the power spectrum

$$S(q)=\langle u(q)u(-q)\rangle\sim q^{-(1-\gamma)}, \tag{1}$$

where $u(q)$ are the Fourier transform coefficients of $u(i)$ and γ is the correlation exponent. Thus, we generate $u(q)$ using the following transformation:

$$u(q)=[S(q)]^{1/2}\eta(q), \tag{2}$$

where $S(q)$ is the desired power spectrum in Eq. (1).

(c) We calculate the inverse Fourier transform of $u(q)$ to obtain $u(i)$.

We use the stationary correlated signal $u(i)$ to generate signals with different types of nonstationarities and apply the DFA method [3] to quantify correlations in these nonstationary signals.

Next, we briefly introduce the DFA method, which involves the following steps [3].

(i) Starting with a correlated signal $u(i)$, where $i=1,\ldots,N_{max}$, and N_{max} is the length of the signal, we first integrate the signal $u(i)$ and obtain $y(k)\equiv\Sigma_{i=1}^{k}[u(i)-\langle u\rangle]$, where $\langle u\rangle$ is the mean.
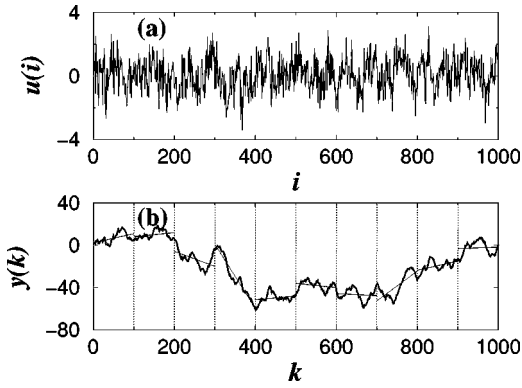
FIG. 1. (a) The correlated signal $u(i)$. (b) The integrated signal $y(k)=\Sigma_{i=1}^{k}[u(i)-\langle u\rangle]$. The vertical dotted lines indicate a box of size $n=100$, the solid straight line segments are the estimated linear "trend" in each box by least-squares fit.

(ii) The integrated signal $y(k)$ is divided into boxes of equal length n.

(iii) In each box of length n, we fit $y(k)$, using a polynomial function of order l, which represents the *trend* in that box. The y coordinate of the fit line in each box is denoted by $y_n(k)$ (see Fig. 1, where linear fit is used). Since we use a polynomial fit of order l, we denote the algorithm as DFA-l.

(iv) The integrated signal $y(k)$ is detrended by subtracting the local trend $y_n(k)$ in each box of length n.

(v) For a given box size n, the root-mean-square (rms) fluctuation for this integrated and detrended signal is calculated:

$$F(n)\equiv\sqrt{\frac{1}{N_{max}}\sum_{k=1}^{N_{max}}[y(k)-y_n(k)]^2}. \qquad (3)$$

(vi) The above computation is repeated for a broad range of scales (box sizes n) to provide a relationship between $F(n)$ and the box size n.

A power-law relation between the average root-mean-square fluctuation function $F(n)$ and the box size n indicates the presence of scaling: $F(n)\sim n^{\alpha}$. The fluctuations can be characterized by a scaling exponent α, a self-similarity parameter that represents the long-range power-law correlation properties of the signal. If $\alpha=0.5$, there is no correlation and the signal is uncorrelated (white noise); if $\alpha<0.5$, the signal is anticorrelated; if $\alpha>0.5$, the signal is correlated [64].

We note that for anticorrelated signals, the scaling exponent obtained from the DFA method overestimates the true correlations at small scales [61]. To avoid this problem, one needs first to integrate the original anticorrelated signal and then apply the DFA method [61]. The correct scaling exponent can thus be obtained from the relation between n and $F(n)/n$ [instead of $F(n)$]. In the following sections, we first integrate the signals under consideration, then apply DFA-2 to remove linear trends in these integrated signals. In order to provide a more accurate estimate of $F(n)$, the largest box size n we use is $N_{max}/10$, where N_{max} is the total number of points in the signal.

We compare the results of the DFA method obtained from the nonstationary signals with those obtained from the stationary signal $u(i)$ and examine how the scaling properties of a detrended fluctuation function $F(n)$ change when introducing different types of nonstationarities.

III. SIGNALS WITH SEGMENTS REMOVED

In this section, we study the effect of nonstationarity caused by removing segments of a given length from a signal and stitching together the remaining parts—a "cutting" procedure often used in preprocessing data prior to analysis. To address this question, we first generate a stationary correlated signal $u(i)$ (see Sec. II) of length N_{max} and a scaling exponent α, using the modified Fourier filtering method [63]. Next, we divide this signal into N_{max}/W nonoverlapping segments of size W and randomly remove some of these segments. Finally, we stitch together the remaining segments in the signal $u(i)$ [Fig. 2(a)], thus obtaining a surrogate nonstationary signal, which is characterized by three parameters: the scaling exponent α, the segment size W, and the fraction of the signal $u(i)$, which is removed.

We find that the scaling behavior of such a nonstationary signal strongly depends on the scaling exponent α of the original stationary correlated signal $u(i)$. As illustrated in Fig. 2(b), for a stationary *anticorrelated* signal with $\alpha=0.1$, the cutting procedure causes a crossover in the scaling behavior of the resultant nonstationary signal. This crossover appears even when only 1% of the segments are cut out. At scales larger than the crossover scale $n_{\times}$, the rms fluctuation function behaves as $F(n)\sim n^{0.5}$, which means an uncorrelated randomness, i.e., the anticorrelation has been completely destroyed in this regime. For all anticorrelated signals with exponent $\alpha<0.5$, we observe a similar crossover behavior. This result is surprising, since researchers often take for granted that a cutting procedure before analysis does not change the scaling properties of the original signal. Our simulation shows that this assumption is not true, at least for anticorrelated signals.

Next, we investigate how the two parameters—the segment size W and the fraction of points cut out from the signal—control the effect of the cutting procedure on the scaling behavior of anticorrelated signals. For a fixed size of the segments ($W=20$), we find that the crossover scale $n_{\times}$ *decreases* with the *increasing* fraction of the cut out segments [Fig. 2(c)]. Furthermore, for anticorrelated signals with small values of the scaling exponent α, e.g., $\alpha=0.1$ and $\alpha=0.2$, we find that $n_{\times}$ and the fraction of the cut out segments display an approximate power-law relationship. For a fixed fraction of the removed segments, we find that the crossover scale $n_{\times}$ *increases* with *increasing* segment size W [Fig. 2(d)]. To minimize the effect of the cutting procedure on the correlation properties, it is advantageous to cut smaller number of segments of larger size W. Moreover, if the segments that need to be removed are too close (e.g., at a distance shorter than the size of the segments), it may be advantageous to cut out both the segments and a part of the signal between them. This will effectively increase the size of the segment W without substantially changing the fraction
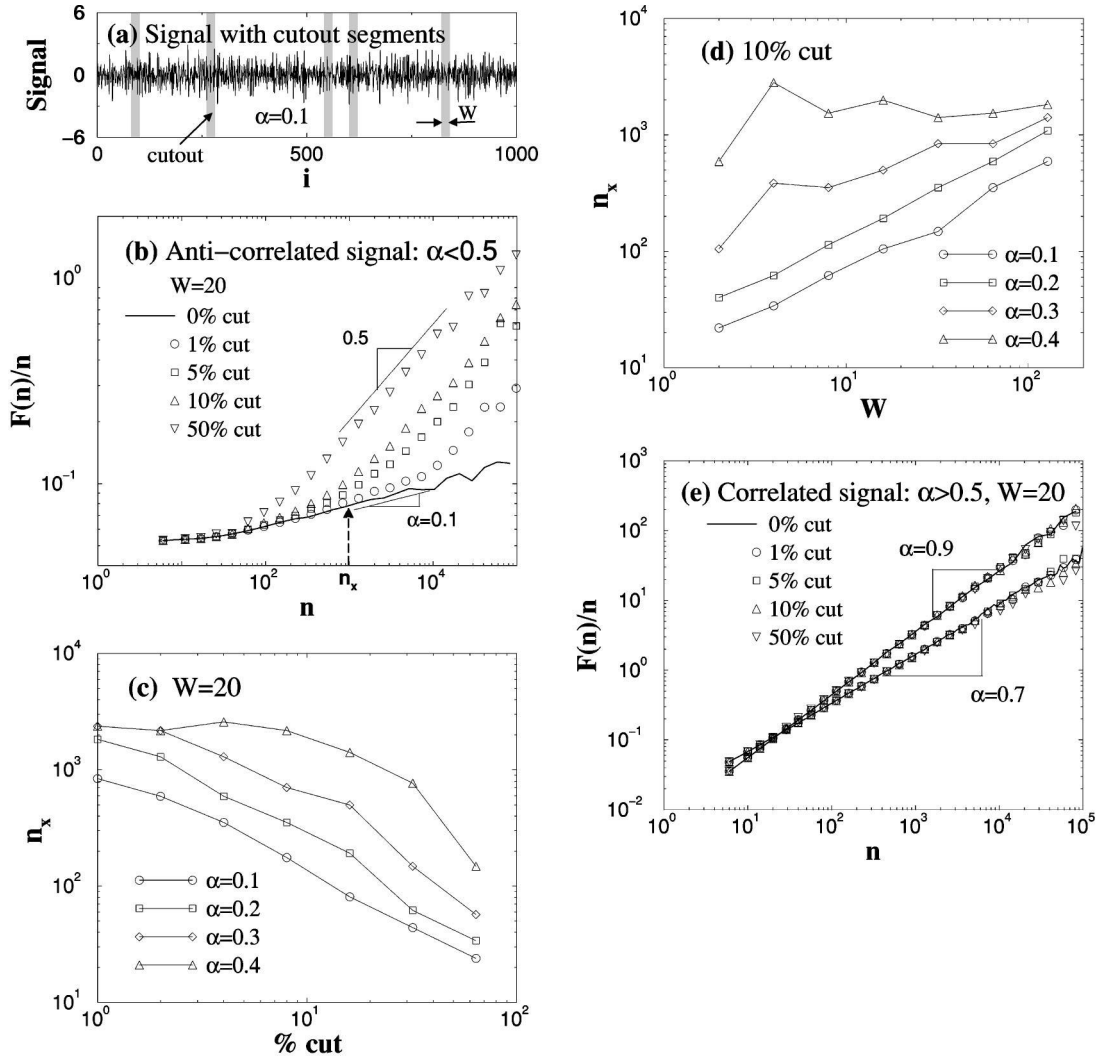
FIG. 2. Effects of the ''cutting'' procedure on the scaling behavior of stationary correlated signals. $N_{max}=2^{20}$ is the number of points in the signals (standard deviation $\sigma=1$) and W is the size of the cut out segments. (a) A stationary signal with 10% of the points removed. The removed parts are presented by shaded segments of size $W=20$ and the remaining parts are stitched together. (b) Scaling behavior of nonstationary signals obtained from an anticorrelated stationary signal (scaling exponent $\alpha<0.5$) after the cutting procedure. A crossover from anticorrelated to uncorrelated ($\alpha=0.5$) behavior appears at scale $n_{\times}$. The crossover scale $n_{\times}$ decreases by increasing the fraction of points removed from the signal. We determine $n_{\times}$ based on the difference Δ between the logarithm of $F(n)/n$ for the original stationary anticorrelated signal ($\alpha=0.1$) and the nonstationary signal with cut out segments: $n_{\times}$ is the scale at which $\Delta\geq0.04$. Dependence of the crossover scale $n_{\times}$ on the fraction (c) and on the size W (d) of the cutout segments for anticorrelated signals with different scaling exponents α. (e) Cutting procedure applied to correlated signals ($\alpha>0.5$). In contrast to (b), no discernible effect on the scaling behavior is observed for different values of the scaling exponent α, even when up to 50% of the points in the signals are removed.

of the signal that is cut out, leading to an increase in the crossover scale $n_{\times}$. Such a strategy would minimize the effect of this type of nonstationarity on the scaling properties of the data. For small values of the scaling exponent α ($\alpha<0.25$), we find that $n_{\times}$ and W follow power-law relationships [Fig. 2(d)]. The reason we do not observe a power-law relationship between $n_{\times}$ and W and between $n_{\times}$ and the fraction of cut out segments, for the values of the scaling exponent α close to 0.5, may be due to the fact that the crossover regime becomes broader when it separates scaling regions with similar exponents, thus leading to an uncertainty in defining $n_{\times}$. For a fixed W and a fixed fraction of

the removed segments [see Figs. 2(c) and 2(d)], we observe that $n_{\times}$ increases with the increasing value of the scaling exponent α, i.e., the effect of the cutting procedure on the scaling behavior decreases when the anticorrelations in the signal are weaker (α closer to 0.5).

Finally, we consider the case of correlated signals $u(i)$ with $1.5>\alpha>0.5$. Surprisingly, we find that the scaling of correlated signals is not affected by the cutting procedure. This observation remains true independently of the segment size W—from very small $W(=5)$ up to very large W ($=5000$) segments—even when up to 50% of the segments are removed from a signal with $N_{max}\sim10^{6}$ points [Fig. 2(e)].

IV. SIGNALS WITH RANDOM SPIKES

In this section, we consider nonstationarity related to the presence of random spikes in the data and we study the effect of this type of nonstationarity on the scaling properties of correlated signals. First, we generate surrogate nonstationary signals by adding random spikes to a stationary correlated signal $u(i)$ [see Sec. II and Figs. 3(a)–3(c)].

We find that the correlation properties of the nonstationary signal with spikes depend on the scaling exponent α of the stationary signal and the scaling exponent α_{sp} of the spikes. When uncorrelated spikes ($\alpha_{sp}=0.5$) are added to a correlated or anticorrelated stationary signal [Figs. 3(d) and 3(e)], we observe a change in the scaling behavior with a crossover at a characteristic scale $n_\times$. For anticorrelated signals ($\alpha < 0.5$) with random spikes, we find that at scales smaller than $n_\times$, the scaling behavior is close to that observed for the stationary anticorrelated signal without spikes, while for scales larger than $n_\times$, there is a crossover to random behavior. In the case of correlated signals ($\alpha > 0.5$) with random spikes, we find a different crossover from uncorrelated behavior at small scales, to correlated behavior at large scales with an exponent close to the exponent of the original stationary correlated signal. Moreover, we find that spikes with a very small amplitude can cause strong crossovers in the case of anticorrelated signals, while for correlated signals, identical concentrations of spikes with a much larger amplitude do not affect the scaling. Based on these findings, we conclude that uncorrelated spikes with a sufficiently large amplitude can affect the DFA results at large scales for signals with $\alpha < 0.5$ and at small scales for signals with $\alpha > 0.5$.

To better understand the origin of this crossover behavior, we first study the scaling of the spikes only [see Fig. 3(b)]. By varying the concentration p ($0 \leq p \leq 1$) and the amplitude A_{sp} of the spikes in the signal, we find that for the general case when the spikes may be correlated, the rms fluctuation function behaves as

$$F_{sp}(n)/n = k_0 \sqrt{p} A_{sp} n^{\alpha_{sp}}, \tag{4}$$

where k_0 is a constant and α_{sp} is the scaling exponent of the spikes.

Next, we investigate the analytical relation between the DFA results obtained from the original correlated signal, the spikes, and the superposition of signal and spikes. Since the original signal and the spikes are not correlated, we can use a *superposition rule* (see [61] and Appendix A) to derive the rms fluctuation function $F(n)/n$ for the correlated signal with spikes,

$$[F(n)/n]^2 = [F_\eta(n)/n]^2 + [F_{sp}(n)/n]^2, \tag{5}$$

where $F_\eta(n)/n$ and $F_{sp}(n)/n$ are the rms fluctuation functions for the signal and the spikes, respectively. To confirm this theoretical result, we calculate $\sqrt{[F_\eta(n)/n]^2 + [F_{sp}(n)/n]^2}$ [see Figs. 3(d) and 3(e)] and find that Eq. (5) is remarkably consistent with our experimental observations.
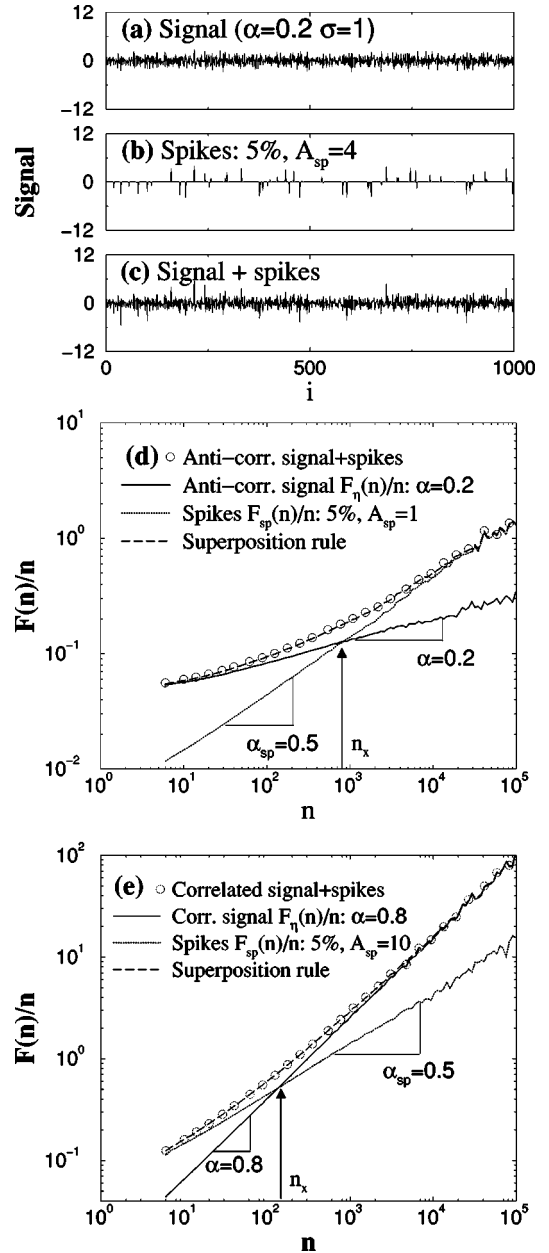

FIG. 3. Effects of random spikes on the scaling behavior of stationary correlated signals. (a) An example of an anticorrelated signal $u(i)$ with scaling exponent $\alpha = 0.2$, $N_{max} = 2^{20}$, and standard deviation $\sigma = 1$. (b) A series of uncorrelated spikes ($\alpha_{sp} = 0.5$) at 5% randomly chosen positions (concentration $p = 0.05$) and with uniformly distributed amplitudes A_{sp} in the interval $[-4,4]$. (c) Superposition of the signals in (a) and (b). (d) Scaling behavior of an anticorrelated signal $u(i)$ ($\alpha = 0.2$) with spikes ($A_{sp} = 1$, $p = 0.05$, $\alpha_{sp} = 0.5$). For $n < n_\times$, $F(n)/n \approx F_\eta(n)/n \sim n^\alpha$, where $F_\eta(n)/n$ is the scaling function of the signal $u(i)$. For $n > n_\times$, $F(n)/n \approx F_{sp}(n)/n \sim n^{\alpha_{sp}}$. (e) Scaling behavior of a correlated signal $u(i)$ ($\alpha = 0.8$) with spikes ($A_{sp} = 10$, $p = 0.05$, $\alpha_{sp} = 0.5$). For $n < n_\times$, $F(n)/n \approx F_{sp}(n)/n \sim n^{\alpha_{sp}}$. For $n > n_\times$, $F(n)/n \approx F_\eta(n)/n \sim n^\alpha$. Note that when $\alpha = \alpha_{sp} = 0.5$, there is no crossover.

Using the superposition rule, we can also theoretically predict the crossover scale $n_\times$ as the intercept between $F_\eta(n)/n$ and $F_{sp}(n)/n$, i.e., where $F_\eta(n_\times) = F_{sp}(n_\times)$. We find that

$$n_\times = \left(\sqrt{p} A_{sp} \frac{k_0}{b_0} \right)^{1/(\alpha - \alpha_{sp})}, \qquad (6)$$

since the rms fluctuation functions for the signal and the spikes are $F_\eta(n)/n = b_0 n^\alpha$ [61] and $F_{sp}(n)/n = k_0 \sqrt{p} A_{sp} n^{\alpha_{sp}}$ [Eq. (4)], respectively. This result predicts the position of the crossover depending on the parameters defining the signal and the spikes.

Our result derived from the superposition rule can be useful to distinguish two cases: (i) the correlated stationary signal and the spikes are independent (e.g., the case when a correlated signal results from the intrinsic dynamics of the system while the spikes are due to external perturbations) and (ii) the correlated stationary signal and the spikes are dependent (e.g., both the signal and the spikes arise from the intrinsic dynamics of the system). In the latter case, the identity in the superposition rule is not correct (see Appendix A).

V. SIGNALS WITH DIFFERENT LOCAL BEHAVIOR

Next, we study the effect of nonstationarities on complex patchy signals where different segments show different local behavior. This type of nonstationarity is very common in real world data [5,8,19,33,62]. Our discussion of signals composed of only two types of segments is limited to two simple cases: (a) different standard deviations and (b) different correlations.

A. Signals with different local standard deviations

Here we consider nonstationary signals comprised of segments with the same local scaling exponent, but different local standard deviations. We first generate a stationary correlated signal $u(i)$ (see Sec. II) with fixed standard deviation $\sigma_1 = 1$. Next, we divide the signal $u(i)$ into nonoverlapping segments of size W. We then randomly choose a fraction p of the segments and amplify the standard deviation of the signal in these segments, $\sigma_2 = 4$ [Fig. 4(a)]. Finally, we normalize the entire signal to global standard deviation $\sigma = 1$ by dividing the value of each point of the signal by $\sqrt{(1-p)\sigma_1^2 + p\sigma_2^2}$.

For nonstationary *anticorrelated* signals ($\alpha < 0.5$) with segments characterized by two different values of the standard deviation, we observe a crossover at scale $n_\times$ [Fig. 4(b)]. For small scales $n < n_\times$, the behavior is anticorrelated with an exponent equal to the scaling exponent α of the original stationary anticorrelated signal $u(i)$. For large scales $n > n_\times$, we find a transition to random behavior with exponent 0.5, indicating that the anticorrelations have been destroyed. The dependence of crossover scale $n_\times$ on the fraction p of segments with larger standard deviation is shown in Fig. 4(c). The dependence is not monotonic because for $p = 0$ and $p = 1$, the local standard deviation is constant throughout the signal, i.e., the signal becomes stationary and
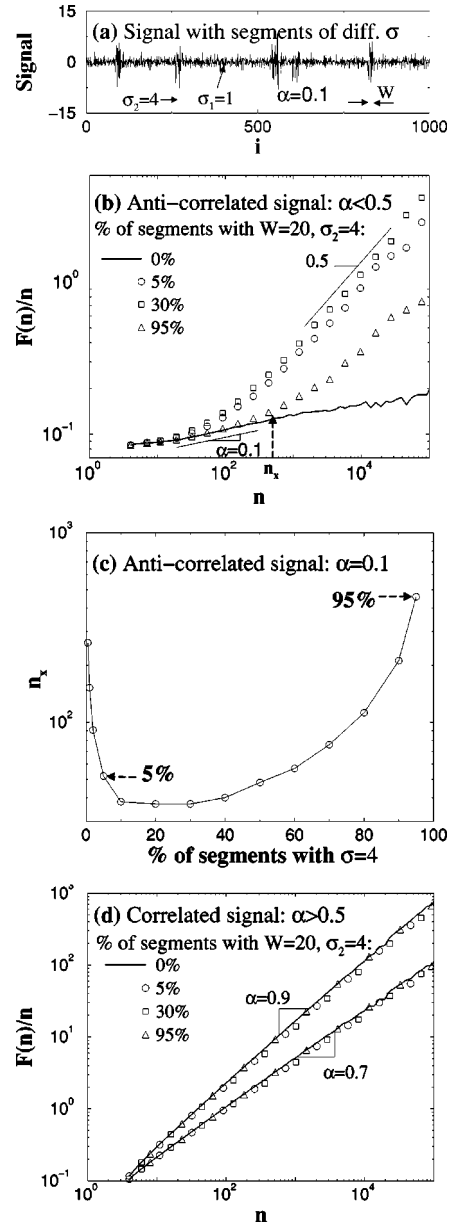
FIG. 4. Scaling behavior of nonstationary correlated signals with different local standard deviations. (a) Anticorrelated signal ($\alpha = 0.1$) with standard deviation $\sigma_1 = 1$ and amplified segments with standard deviation $\sigma_2 = 4$. The size of each segment is $W = 20$ and the fraction of the amplified segments is $p = 0.1$ from the total length of the signal ($N_{max} = 2^{20}$). (b) Scaling behavior of the signal in (a) for a different fraction p of the amplified segments (after normalization of the globe standard deviation to unity). A crossover from anticorrelated behavior ($\alpha = 0.1$) at small scales to random behavior ($\alpha = 0.5$) at large scales is observed. (c) Dependence of the crossover scale $n_\times$ on the fraction p of amplified segments for the signal in (a). $n_\times$ is determined from the difference Δ of $\log_{10}[F(n)/n]$ between the nonstationary signal with amplified segments and the original stationary signal. Here we choose $\Delta = 0.04$. (d) Scaling behavior of nonstationary signals obtained from correlated stationary signals ($1 > \alpha > 0.5$) with standard deviation $\sigma_1 = 1$ for a different fraction of the amplified segments with $\sigma_2 = 4$. No difference in the scaling is observed, compared to the original stationary signal.

thus there is no crossover. Note the asymmetry in the value of $n_\times$—a much smaller value of $n_\times$ for $p = 0.05$ compared to $p = 0.95$ [see Figs. 4(b) and 4(c)]. This result indicates that very few segments with a large standard deviation (compared to the rest of the signal) can have a strong effect on the anticorrelations in the signal. Surprisingly, the same fraction of segments with a small standard deviation (compared to the rest of the signal) does not affect the anticorrelations up to relatively large scales.

For nonstationary *correlated* signals ($\alpha > 0.5$) with segments characterized by two different values of the standard deviation, we surprisingly find no difference in the scaling of $F(n)/n$, compared to the stationary correlated signals with constant standard deviation [Fig. 4(d)]. Moreover, this observation remains valid for different sizes of the segments W and for different values of the fraction p of segments with larger standard deviation. We note that in the limiting case of very large values of σ_2/σ_1, when the values of the signal in the segments with standard deviation σ_1 could be considered close to "zero," the results in Fig. 4(d) do not hold and we observe a scaling behavior similar to that of the signal in Fig. 5(c) (see following section).

B. Signals with different local correlations

Next we consider nonstationary signals that consist of segments with identical standard deviations ($\sigma = 1$) but different correlations. We obtain such signals using the following procedure: (1) generate two stationary signals $u_1(i)$ and $u_2(i)$ (see Sec. II) of identical length N_{max} and with different correlations, characterized by scaling exponents α_1 and α_2; (2) divide the signals $u_1(i)$ and $u_2(i)$ into nonoverlapping segments of size W; (3) randomly replace a fraction p of the segments in signal $u_1(i)$ with the corresponding segments of $u_2(i)$. In Fig. 5(a), we show an example of such a complex nonstationary signal with different local correlations. In this section, we study the behavior of the rms fluctuation function $F(n)/n$. We also investigate $F(n)/n$ separately for each component of the nonstationary signal (which consists only of the segments with identical local correlations) and suggest an approach, based on the DFA results, to recognize such complex structures in real data.

In Fig. 5(d), we present the DFA result on such a nonstationary signal, composed of segments with two different types of local correlations characterized by exponents $\alpha_1 = 0.1$ and $\alpha_2 = 0.9$. We find that at small scales the slope of $F(n)/n$ is close to α_1 and at large scales the slope approaches α_2 with a bump in the intermediate scale regime. This is not surprising since $\alpha_1 < \alpha_2$ and thus $F(n)/n$ is bound to have a small slope (α_1) at small scales and a large slope (α_2) at large scales. However, it is surprising that although 90% of the signal consists of segments with scaling exponent α_1, $F(n)/n$ deviates at small scales ($n \approx 10$) from the behavior expected for an anticorrelated signal $u(i)$ with exponent α_1 [see, e.g., the solid line in Fig. 2(b)]. This suggests that the behavior of $F(n)/n$ for a nonstationary signal comprised of mixed segments with different correlations is dominated by segments exhibiting higher positive correlations even in the case when their relative fraction in the
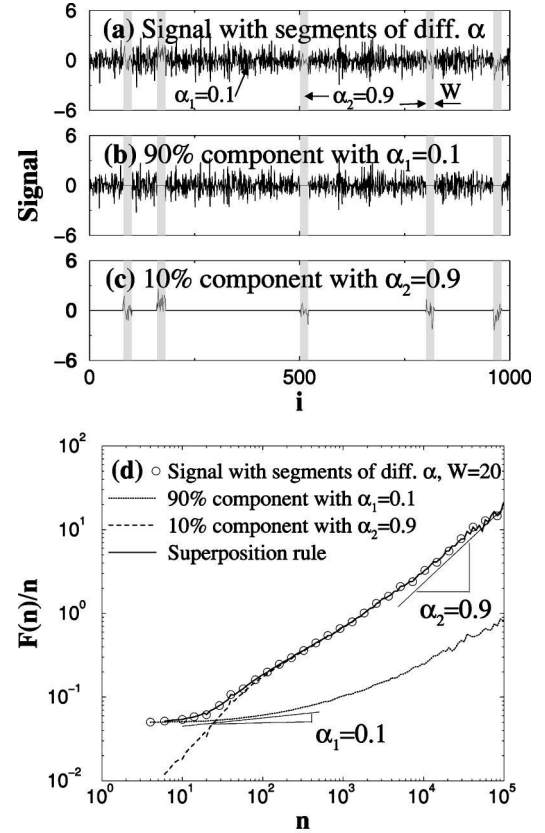

FIG. 5. Scaling behavior of a nonstationary signal with two different scaling exponents. (a) Nonstationary signal (length $N_{max} = 2^{20}$, standard deviation $\sigma = 1$), which is a mixture of correlated segments with exponent $\alpha_1 = 0.1$ (90% of the signal) and segments with exponent $\alpha_2 = 0.9$ (10% of the signal). The segment size is $W = 20$, (b) the 90% component containing all segments with $\alpha_1 = 0.1$ and the remaining segments (with $\alpha_2 = 0.9$) are replaced by zero, (c) the 10% component containing all segments with $\alpha_2 = 0.9$ and the remaining segments (with $\alpha_1 = 0.1$) are replaced by zero, (d) DFA results for the mixed signal in (a), for the individual components in (b) and (c), and our prediction obtained from the superposition rule.

signal is small. This observation is pertinent to real data such as (i) heart rate recordings during sleep where different segments corresponding to different sleep stages exhibit different types of correlations [33], (ii) DNA sequences including coding and noncoding regions characterized by different correlations [5,8,16], and (iii) brain wave signals during different sleep stages [62].

To better understand the complex behavior of $F(n)/n$ for such nonstationary signals, we study their components separately. Each component is composed only of those segments in the original signal that are characterized by identical correlations, while the segments with different correlations are substituted with zeros [see Figs. 5(b) and 5(c)]. Since the two components of the nonstationary signal in Fig. 5(a) are independent, based on the superposition rule [Eq. (5)], we expect that the rms fluctuation function $F(n)/n$ will behave as $\sqrt{[F_1(n)/n]^2 + [F_2(n)/n]^2}$, where $F_1(n)/n$ and $F_2(n)/n$ are the rms fluctuation functions of the components in Figs. 5(b)

and 5(c), respectively. We find a remarkable agreement between the superposition rule prediction and the result of the DFA method obtained directly from the mixed signal [Fig. 5(d)]. This finding helps us understand the relation between the scaling behavior of the mixed nonstationary signal and its components.

Information on the effect of such parameters as the scaling exponents α_1 and α_2, the size of the segments W, and their relative fraction p on the scaling behavior of the components provides insight into the scaling behavior of the original mixed signal. When the original signal comes from real data, its composition is *a priori* unknown. A first step is to "guess" the type of correlations (exponents α_1 and α_2) present in the signal, based on the scaling behavior of $F(n)/n$ at small and large scales [Fig. 5(d)]. A second step is to determine the parameters W and p for each component by matching the scaling result from the superposition rule with the original signal. Hence in the following sections, we focus on the scaling properties of the components and how they change with p, α, and W.

1. Dependence on the fraction of segments

First, we study how the correlation properties of the components depend on the fraction p of the segments with identical local correlations. For components containing segments with anticorrelations ($0 < \alpha < 0.5$) and fixed size W [Fig. 5(b)], we find a crossover to random behavior ($\alpha = 0.5$) at large scales, which becomes more pronounced (shift to smaller scales) when the fraction p decreases [Fig. 6(a)]. At *small* scales ($n \leq W$), the slope of $F(n)/n$ is identical to that expected for a stationary signal $u(i)$ (i.e., $p = 1$) with the same anticorrelations [solid line in Fig. 6(a)]. Moreover, we observe a vertical shift in $F(n)/n$ to lower values when the fraction p of nonzero anticorrelated segments decreases. We find that at small scales, after rescaling $F(n)/n$ by $\sqrt{p}$, all curves collapse on the curve for the stationary anticorrelated signal $u(i)$ [Fig. 6(a)]. Since at small scales ($n \leq W$) the behavior of $F(n)/n$ does not depend on the segment size W, this collapse indicates that the vertical shift in $F(n)/n$ is due only to the fraction p. Thus, to determine the fraction p of anticorrelated segments in a nonstationary signal [mixture of anticorrelated and correlated segments, Fig. 5(a)] we only need to estimate at small scales the vertical shift in $F(n)/n$ between the mixed signal [Fig. 5(d)] and a stationary signal $u(i)$ with identical anticorrelations. This approach is valid for nonstationary signals where the fraction p of the anticorrelated segments is much larger than the fraction of the correlated segments in the mixed signal [Fig. 5(a)], since only under this condition the anticorrelated segments can dominate $F(n)/n$ of the mixed signal at small scales [Fig. 5(d)].

For components containing segments with positive correlations ($0.5 < \alpha < 1$) and fixed size W [Fig. 5(c)], we observe a similar behavior for $F(n)/n$, with collapse at *small* scales ($n \leq W$) after rescaling by $\sqrt{p}$ [Fig. 6(b)] (for $\alpha > 1$, there are exceptions with different rescaling factors, see Appendix B). At small scales the values of $F(n)/n$ for components containing segments with positive correlations are much larger compared to the values of $F(n)/n$ for components containing
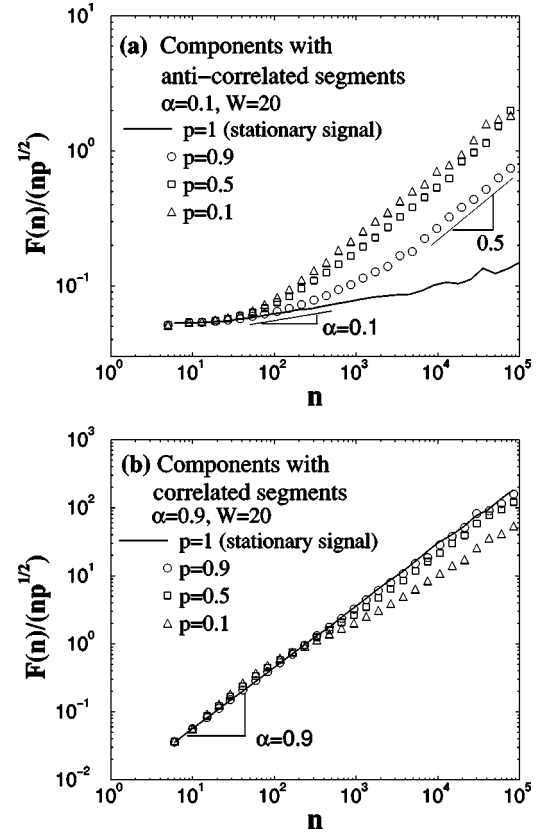

FIG. 6. Dependence of the scaling behavior of components on the fraction p of the segments with identical local correlations, emphasizing data collapse at *small* scales. The segment size is $W = 20$ and the length of the components is $N_{max} = 2^{20}$. (a) Components containing anticorrelated segments ($\alpha = 0.1$) at *small* scales ($n \leq W$). The slope of $F(n)/n$ is identical to that expected for a stationary ($p = 1$) signal with the same anticorrelations. After rescaling $F(n)/n$ by $\sqrt{p}$, at small scales all curves collapse on the curve for the stationary anticorrelated signal. (b) Components containing correlated segments ($\alpha = 0.9$) at *small* scales ($n \leq W$). The slope of $F(n)/n$ is identical to that expected for a stationary ($p = 1$) signal with the same correlations. After rescaling $F(n)/n$ by $\sqrt{p}$, at small scales all curves collapse on the curve for the stationary correlated signal.

an identical fraction p of anticorrelated segments [Fig. 6(a)]. Thus, for a mixed signal where the fraction of correlated segments is not too small (e.g., $p \geq 0.2$), the contribution at small scales of the anticorrelated segments to $F(n)/n$ of the mixed signal [Fig. 5(d)] may not be observed, and the behavior (values and slope) of $F(n)/n$ will be dominated by the correlated segments. In this case, we must consider the behavior of $F(n)/n$ of the mixed signal at large scales only, since the contribution of the anticorrelated segments at large scales is negligible. Hence, we next study the scaling behavior of components with correlated segments at *large* scales.

For components containing segments with positive correlations and fixed size W [Fig. 5(c)], we find that at *large* scales the slope of $F(n)/n$ is identical to that expected for a stationary signal $u(i)$ (i.e., $p = 1$) with the same correlations [solid line in Fig. 7(a)]. We also observe a vertical shift in $F(n)/n$ to lower values when the fraction p of nonzero cor-
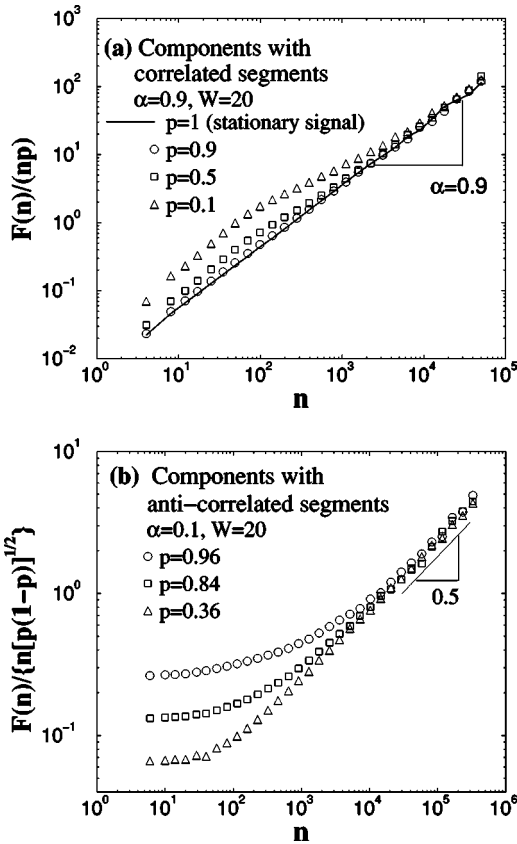
FIG. 7. Dependence of scaling behavior of components on the fraction p of the segments with identical local correlations, emphasizing data collapse at *large* scales. The segment size is $W=20$ and the length of the components is $N_{max}=2^{20}$. (a) Components containing correlated segments ($\alpha=0.9$) at *large* scales ($n \gg W$). The slope of $F(n)/n$ is identical to that expected for a stationary ($p=1$) signal with the same correlations. After rescaling $F(n)/n$ by p, at large scales all curves collapse on the curve for the stationary correlated signal. (b) Components containing anticorrelated segments ($\alpha=0.1$) at *large* scales ($n \gg W$). There is a crossover to random behavior ($\alpha=0.5$). After rescaling $F(n)/n$ by $\sqrt{p(1-p)}$, all curves collapse at large scales.

related segments in the component decreases. We find that after rescaling $F(n)/n$ by p, at large scales all curves collapse on the curve representing the stationary correlated signal $u(i)$ [Fig. 7(a)]. Since at large scales ($n \gg W$), the effect of the zero segments of size W on the rms fluctuation function $F(n)/n$ for components with correlated segments is negligible, even when the zero segments are 50% of the component [see Fig. 7(a)], the finding of a collapse at large scales indicates that the vertical shift in $F(n)/n$ is only due to the fraction p of the correlated segments. Thus, to determine the fraction p of correlated segments in a nonstationary signal (which is a mixture of anticorrelated and correlated segments [Fig. 5(a)]), we only need to estimate at large scales the vertical shift in $F(n)/n$ between the mixed signal [Fig. 5(d)] and a stationary signal $u(i)$ with identical correlations.

For components containing segments with anticorrelations and fixed size W [Fig. 5(b)], we find that at large scales in order to collapse the $F(n)/n$ curves ($n \gg W$) [Fig. 6(a)] we

need to rescale $F(n)/n$ by $\sqrt{p(1-p)}$ [see Fig. 7(b)]. Note that there is a difference between the rescaling factors for components with anticorrelated and correlated segments at small [Figs. 6(a)–6(b)] and large [Figs. 7(a)–7(b)] scales. We also note that for components with correlated segments ($\alpha > 0.5$) and sufficiently small p, there is a different rescaling factor of $\sqrt{p(1-p)}$ in the intermediate scale regime (see Appendix B, Fig. 10).

For components containing segments of white noise ($\alpha=0.5$), we find no change in the scaling exponent as a function of the fraction p of the segments, i.e., $\alpha=0.5$ for the components at both small and large scales. However, we observe at all scales a vertical shift in $F(n)/n$ to lower values with decreasing p: $F(n)/n \sim \sqrt{p}$.

2. Dependence on the size of segments

Next, we study how the scaling behavior of the components depends on the size of the segments W. First, we consider components containing segments with anticorrelations. For a fixed value of the fraction p of the segments, we study how $F(n)/n$ changes with W. At small scales, we observe a behavior with a slope similar to that for a stationary signal $u(i)$ with identical anticorrelations [Fig. 8(a)]. At large scales, we observe a crossover to random behavior (exponent $\alpha=0.5$) with an increasing crossover scale when W increases. At large scales, we also find a vertical shift with increasing values of $F(n)/n$ when W decreases [Fig. 8(a)]. Moreover, we find that there is an equidistant vertical shift in $F(n)/n$ when W decreases by a factor of 10, suggesting a power-law relation between $F(n)/n$ and W at large scales.

For components containing correlated segments with a fixed value of the fraction p we find that in the intermediate scale regime, the segment size W plays an important role in the scaling behavior of $F(n)/n$ [Fig. 8(b)]. We first focus on the intermediate scale regime when both $p=0.1$ and $W=20$ are fixed [middle curve in Fig. 8(b)]. We find that for a small fraction p of the correlated segments, $F(n)/n$ has slope $\alpha=0.5$, indicating random behavior [Fig. 8(b)], which shrinks when p increases (see Appendix B, Fig. 10). Thus, for components containing correlated segments, $F(n)/n$ approximates at large and small scales the behavior of a stationary signal with identical correlations ($\alpha=0.9$), while in the intermediate scale regime there is a plateau of random behavior due to the random "jumps" at the borders between the nonzero and zero segments [Fig. 5(c)]. Next, we consider the case when the fraction of correlated segments p is fixed while the segment size W changes. We find a vertical shift with increasing values for $F(n)/n$ when W increases [Fig. 8(b)], as opposed to what we observe for components with anticorrelated segments [Fig. 8(a)]. Since the vertical shift in $F(n)/n$ is equidistant when W increases by a factor of 10, our finding indicates a power-law relationship between $F(n)/n$ and W.

3. Scaling expressions

To better understand the complexity in the scaling behavior of components with correlated and anticorrelated seg-
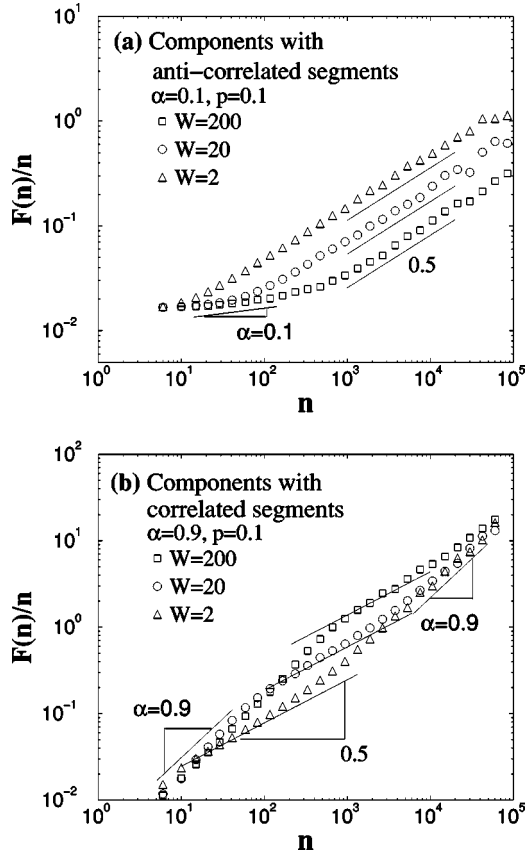
FIG. 8. Dependence of the scaling behavior of components on the segment size W. The fraction $p=0.1$ of the nonzero segments is fixed and the length of the components is $N_{max}=2^{20}$. (a) Components containing anticorrelated segments ($\alpha=0.1$). At large scales ($n \gg W$), there is a crossover to random behavior ($\alpha=0.5$). An equidistant vertical shift in $F(n)/n$ when W decreases by a factor of 10 suggests a power-law relation between $F(n)/n$ and W. (b) Components containing correlated segments ($\alpha=0.9$). At intermediate scales, $F(n)/n$ has slope $\alpha=0.5$, indicating random behavior. An equidistant vertical shift in $F(n)/n$ suggests a power-law relation between $F(n)/n$ and W.

ments at different scales, we employ the superposition rule (see [61] and Appendix A). For each component we have

$$F(n)/n = \sqrt{[F_{\text{corr}}(n)/n]^2 + [F_{\text{rand}}(n)/n]^2}, \quad (7)$$

where $F_{\text{corr}}(n)/n$ accounts for the contribution of the correlated or anticorrelated nonzero segments and $F_{\text{rand}}(n)/n$ accounts for the randomness due to "jumps" at the borders between nonzero and zero segments in the component.

Components with correlated segments ($\alpha > 0.5$). At small scales $n < W$, our findings presented in Fig. 6(b) suggest that there is no substantial contribution from $F_{\text{rand}}(n)/n$. Thus from Eq. (7),

$$F(n)/n \approx F_{\text{corr}}(n)/n \sim b_0 \sqrt{p} n^\alpha, \quad (8)$$

where $b_0 n^\alpha$ is the rms fluctuation function for stationary ($p=1$) correlated signals [Eq. (6) and [61]].

Similarly, at large scales $n \gg W$, we find that the contribution of $F_{\text{rand}}(n)/n$ is negligible [see Fig. 7(a)], thus from Eq. (7) we have

$$F(n)/n \approx F_{\text{corr}}(n)/n \sim b_0 p n^\alpha. \quad (9)$$

However, in the intermediate scale regime, the contribution of $F_{\text{rand}}(n)/n$ to $F(n)/n$ is substantial. To confirm this we use the superposition rule [Eq. (7)] and our estimates for $F_{\text{corr}}(n)/n$ at small [Eq. (8)] and large [Eq. (9)] scales [65]. The result we obtain from

$$F_{\text{rand}}(n)/n = \sqrt{[F(n)/n]^2 - [b_0\sqrt{p}n^\alpha]^2 - [b_0 p n^\alpha]^2} \quad (10)$$

overlaps with $F(n)/n$ in the intermediate scale regime, exhibiting a slope of ≈ 0.5: $F_{\text{rand}}(n)/n \sim n^{0.5}$ [Fig. 9(a)]. Thus, $F_{\text{rand}}(n)/n$ is indeed a contribution due to the random jumps between the nonzero correlated segments and the zero segments in the component [see Fig. 5(c)].

Further, our results in Fig. 8(b) suggest that in the intermediate scale regime, $F(n)/n \sim W^{g_c(\alpha)}$ for fixed fraction p (see Sec. VB 2), where the power-law exponent $g_c(\alpha)$ may be a function of the scaling exponent α characterizing the correlations in the nonzero segments. Since at intermediate scales $F_{\text{rand}}(n)/n$ dominates the scaling [Eq. (10) and Fig. 9(a)], from Eq. (7) we find $F_{\text{rand}}(n)/n \approx F(n)/n \sim W^{g_c(\alpha)}$. We also find that at intermediate scales, $F(n)/n \sim \sqrt{p(1-p)}$ for fixed segment size W (see Appendix B, Fig. 10). Thus from Eq. (7) we find $F_{\text{rand}}(n)/n \approx F(n)/n \sim \sqrt{p(1-p)}$. Hence we obtain the following general expression:

$$F_{\text{rand}}(n)/n \sim h(\alpha)\sqrt{p(1-p)} W^{g_c(\alpha)} n^{0.5}. \quad (11)$$

Here we assume that $F_{\text{rand}}(n)/n$ also depends directly on the type of correlations in the segments through some function $h(\alpha)$.

To determine the form of $g_c(\alpha)$ in Eq. (11), we perform the following steps.

(a) We fix the values of p and α, and from Eq. (10) we calculate the value of $F_{\text{rand}}(n)/n$ for two different values of the segment size W, e.g., we choose $W_1=400$ and $W_2=20$.

(b) From the expression in Eq. (11), at the same scale n in the intermediate scale regime, we determine the ratio

$$F_{\text{rand}}(W_1)/F_{\text{rand}}(W_2) = (W_1/W_2)^{g_c(\alpha)}. \quad (12)$$

(c) We plot $F_{\text{rand}}(W_1)/F_{\text{rand}}(W_2)$ vs α on a linear-log scale [Fig. 9(b)]. From the graph and Eq. (12) we obtain the dependence

$$g_c(\alpha) = \frac{\ln[F_{\text{rand}}(W_1)/F_{\text{rand}}(W_2)]}{\ln(W_1/W_2)}$$

$$= \begin{cases} C\alpha - C/2, & 0.5 \leq \alpha \leq 1 \\ 0.50 & \text{for} \quad \alpha > 1, \end{cases} \quad (13)$$

where $C=0.87 \pm 0.06$. Note that $g_c(0.5)=0$.

To determine if $F_{\text{rand}}(n)/n$ depends on $h(\alpha)$ in Eq. (11), we perform the following steps.
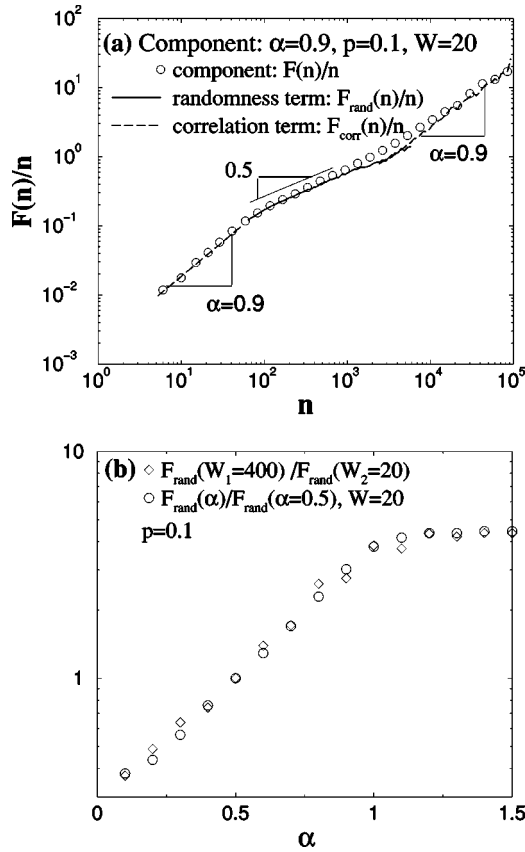
FIG. 9. (a) Scaling behavior of components containing correlated segments ($\alpha > 0.5$). $F(n)/n$ exhibits two crossovers and three scaling regimes at small, intermediate, and large scales. From the superposition rule [Eq. (7)] we find that the small and large scale regimes are controlled by the correlations ($\alpha = 0.9$) in the segments [$F_{\text{corr}}(n)/n$ from Eqs. (8) and (9)] while the intermediate regime [$F_{\text{rand}}(n)/n \sim n^{0.5}$ from Eq. (10)] is dominated by the random jumps at the borders between nonzero and zero segments. (b) The ratio $F_{\text{rand}}(W_1 = 400)/F_{\text{rand}}(W_2 = 20)$ in the intermediate scale regime for fixed p and different values of α, and the ratio $F_{\text{rand}}(\alpha)/F_{\text{rand}}(\alpha = 0.5)$ for fixed p and $W \equiv W_1/W_2$. $F_{\text{rand}}(n)/n$ is obtained from Eq. (10) and the ratios are estimated for all scales n in the intermediate regime. The two curves overlap for a broad range of values for the exponent α, suggesting that $F_{\text{rand}}(n)/n$ does not depend on $h(\alpha)$ [see Eqs. (11) and (16)].

(a) We fix the values of p and W and calculate the value of $F_{\text{rand}}(n)/n$ for two different values of the scaling exponent α, e.g., 0.5 and any other value of α from Eq. (10).

(b) From the expression in Eq. (11), at the same scale n in the intermediate scale regime, we determine the ratio

$$\frac{F_{\text{rand}}(\alpha)}{F_{\text{rand}}(0.5)} = \frac{h(\alpha)}{h(0.5)} W^{g_c(\alpha) - g_c(0.5)} = \frac{h(\alpha)}{h(0.5)} W^{g_c(\alpha)}, \tag{14}$$

since $g_c(0.5) = 0$ from Eq. (13).

(c) We plot $F_{\text{rand}}(\alpha)/F_{\text{rand}}(0.5)$ vs α on a linear-log scale [Fig. 9(b)] and find that when $W \equiv W_1/W_2$ [in Eqs. (12) and (14)] this curve overlaps with $F_{\text{rand}}(W_1)/F_{\text{rand}}(W_2)$ vs α

[Fig. 9(b)] for all values of the scaling exponent $0.5 \leq \alpha \leq 1.5$. From this overlap and from Eqs. (12) and (14), we obtain

$$W^{g_c(\alpha)} = \frac{h(\alpha)}{h(0.5)} W^{g_c(\alpha)} \tag{15}$$

for every value of α, suggesting that $h(\alpha) = \text{const}$ and thus $F_{\text{rand}}(n)/n$ can finally be expressed as

$$F_{\text{rand}}(n)/n \sim \sqrt{p(1-p)} W^{g_c(\alpha)} n^{0.5}. \tag{16}$$

Components with anticorrelated segments ($\alpha < 0.5$). Our results in Fig. 6(a) suggest that at small scales $n < W$ there is no substantial contribution of $F_{\text{rand}}(n)/n$ and that

$$F(n)/n \approx F_{\text{corr}}(n)/n \sim b_0 \sqrt{p} \, n^{\alpha}, \tag{17}$$

a behavior similar to the one we find for components with correlated segments [Eq. (8)].

In the intermediate and large scale regimes ($n \geq W$), from the plots in Figs. 7(b) and 8(a) we find that the scaling behavior of $F(n)/n$ is controlled by $F_{\text{rand}}(n)/n$ and thus

$$F(n)/n \approx F_{\text{rand}}(n)/n \sim \sqrt{p(1-p)} W^{g_a(\alpha)} n^{0.5}, \tag{18}$$

where $g_a(\alpha) = C\alpha - C/2$ for $0 < \alpha < 0.5$ [see Fig. 9(b)], and the relation for $F_{\text{rand}}(n)/n$ is obtained using the same procedure we followed for Eq. (16).

VI. CONCLUSIONS

In this paper we studied the effects of three different types of nonstationarities using the DFA correlation analysis method. Specifically, we consider sequences formed in three ways: (i) stitching together segments of signals obtained from discontinuous experimental recordings, or removing some noisy and unreliable segments from continuous recordings and stitching together the remaining parts; (ii) adding random outliers or spikes to a signal with known correlations, and (iii) generating a signal composed of segments with different properties, e.g., different standard deviations or different correlations. We compare the difference between the scaling results obtained for stationary correlated signals and for correlated signals with artificially imposed nonstationarities.

(i) We find that removing segments from a signal and stitching together the remaining parts does not affect the scaling behavior of positively correlated signals ($1.5 \geq \alpha > 0.5$); even when up to 50% of the points in these signals are removed. However, such a cutting procedure strongly affects anticorrelated signals, leading to a crossover from an anticorrelated regime (at small scales) to an uncorrelated regime (at large scales). The crossover scale $n_\times$ increases with increasing value of the scaling exponent α for the original stationary anticorrelated signal. It also depends both on the segment size and the fraction of the points cut out from the signal: (1) $n_\times$ decreases with the increasing fraction of cut out segments and (2) $n_\times$ increases with increasing segment size. Based on our findings, we propose an approach to mini-

mize the effect of the cutting procedure on the correlation properties of a signal: When two segments that need to be removed are on distances shorter than the size of the segment, it is advantageous to cut out both the segments and the part of the signal between them.

(ii) Signals with superposed random spikes. We find that for an anticorrelated signal with superposed spikes at small scales, the scaling behavior is close to that of the stationary anticorrelated signal without spikes. At large scales, there is a crossover to random behavior. For a correlated signal with spikes, we find a different crossover from uncorrelated behavior at small scales to correlated behavior at large scales with an exponent close to the exponent of the original stationary signal. We also find that the spikes with identical density and amplitude may have a strong effect on the scaling of an anticorrelated signal while they have a much smaller or no effect on the scaling of a correlated signal—when the two signals have the same standard deviations. We investigate the characteristics of the scaling of the spikes only and find that the scaling behavior of the signal with random spikes is a superposition of the scaling of the signal and the scaling of the spikes. We analytically prove this superposition relation by introducing a *superposition rule*.

(iii) Signals composed of segments with different local properties. We find the following.

(a) For nonstationary correlated signals comprised of segments that are characterized by two different values of the standard deviation, there is no difference in the scaling behavior compared to stationary correlated signals with constant standard deviation. For nonstationary anticorrelated signals, we find a crossover at scale $n_\times$. For small scales $n < n_\times$, the scaling behavior is similar to that of the stationary anticorrelated signals with constant standard deviation. For large scales $n > n_\times$, there is a transition to random behavior. We also find that very few segments with large standard deviation can strongly affect the anticorrelations in the signal. In contrast, the same fraction of segments with standard deviation smaller than the standard deviation of the rest of the anticorrelated signal has much weaker effect on the scaling behavior—$n_\times$ is shifted to larger scales.

(b) For nonstationary signals consisting of segments with different correlations, the scaling behavior is a superposition of the scaling of the different components—where each component contains only the segments exhibiting identical correlations and the remaining segments are replaced by zero. Based on our findings, we propose an approach to identify the composition of such complex signals: A first step is to "guess" the type of correlations from the DFA results at small and large scales. A second step is to determine the parameters defining the components, such as the segment size and the fraction of nonzero segments. We studied how the scaling characteristics of the components depend on these parameters and provide analytic scaling expressions.

APPENDIX A: SUPERPOSITION RULE

Here we show how the DFA results for any two signals f and g [denoted as $F_f(n)$ and $F_g(n)$] relate with the DFA result for the sum of these two signals $f+g$ [denoted as $F_{f+g}(n)$, where n is the box length (scale of analysis)]. In the general cases, we find $|F_f - F_g| \leqslant F_{f+g} \leqslant F_f + F_g$. When the two signals are not correlated, we find that the following *superposition rule* is valid: $F_{f+g}^2 = F_f^2 + F_g^2$. Here we derive these relations.

First we summarize again the procedure of the DFA method [3]. It includes the following steps: starting with an original signal $u(i)$ of length N_{max}, we integrate and obtain $y(k) = \sum_{j=1}^{k} [u(j) - \langle u \rangle]$, where $\langle u \rangle$ is the mean of $u(i)$. Next, we divide $y(k)$ into nonoverlapping boxes of equal length n. In each box we fit the signal $y(k)$ using a polynomial function $y_n(k) = a_0 + a_1 x(k) + a_2 x^2(k) + \cdots + a_s x^s(k)$, where $x(k)$ is the x coordinate corresponding to the kth signal point. We calculate the rms fluctuation function $F(n) = \sqrt{(1/N_{max}) \sum_{k=1}^{N_{max}} [y(k) - y_n(k)]^2}$.

To prove the superposition rule, we first focus on one particular box along the signal. In order to find the analytic expression of best fit in this box, we write

$$I(a_0, \ldots, a_s) = \sum_{k=1}^{n} \{y(k) - [a_0 + \cdots + a_s x^s(k)]\}^2, \tag{A1}$$

where $a_m, m = 0, \ldots, s$, are the same for all points in this box. The "best fit" requires that $a_m, m = 0, \ldots, s$ satisfy

$$\frac{\partial I}{\partial a_m} = 0, \quad m = 0, \ldots, s. \tag{A2}$$

Combining Eq. (A1) with Eq. (A2) we obtain $s + 1$ equations

$$y_m = a_0 t_{m0} + a_1 t_{m1} + \cdots + a_s t_{ms}, \quad m = 0, \ldots, s, \tag{A3}$$

where

$$y_m = \sum_{k=1}^{n} y(k) x^m(k), \quad t_{mj} = \sum_{k=1}^{n} x^{m+j}(k), \quad j = 0, \ldots, s. \tag{A4}$$

From Eqs. (A3) we determine $a_0, a_1, \ldots, a_s$.

For the signals f, g, and $f+g$, after the integration in each box we have

$$f_m = a_0 t_{m0} + a_1 t_{m1} + \cdots + a_s t_{ms}, \quad m = 0, \ldots, s,$$

$$g_m = a_0' t_{m0} + a_1' t_{m1} + \cdots + a_s' t_{ms}, \quad m = 0, \ldots, s,$$

$$(f+g)_m = a_0'' t_{m0} + a_1'' t_{m1} + \cdots + a_s'' t_{ms}, \quad m = 0, \ldots, s, \tag{A5}$$

where f_m, g_m, and $(f+g)_m$ correspond to y_m in Eqs. (A3).

Comparing the three groups of equations in Eqs. (A5), we find that when we add the first two groups together, the left side becomes $f_m+g_m=(f+g)_m$, which is precisely the left side of the third group of equations. Thus we find

$$a''_m=a_m+a'_m, \quad m=0,\dots,s \tag{A6}$$

and for each point k in every box, the polynomial fits for the signals f, g, and $f+g$ satisfy

$$(f+g)_n(k)=f_n(k)+g_n(k). \tag{A7}$$

This result can be extended to all boxes in the signals. For the signal $f+g$ we obtain

$$F^2_{f+g}=\frac{1}{N_{max}}\sum_{k=1}^{N_{max}}[f(k)-f_n(k)]^2+[g(k)-g_n(k)]^2$$
$$+2[f(k)-f_n(k)][g(k)-g_n(k)]. \tag{A8}$$

After the substitutions $f(k)-f_n(k)=Y_f(k)$ and $g(k)-g_n(k)=Y_g(k)$, we rewrite the above equation as

$$F^2_{f+g}=\frac{1}{N_{max}}\left[\sum_{k=1}^{N_{max}}[Y_f(k)]^2+\sum_{k=1}^{N_{max}}[Y_g(k)]^2\right.$$
$$\left.+2\sum_{k=1}^{N_{max}}Y_f(k)Y_g(k)\right]=F^2_f+F^2_g$$
$$+\frac{2}{N_{max}}\sum_{k=1}^{N_{max}}Y_f(k)Y_g(k). \tag{A9}$$

In the general case, we can utilize the Cauchy inequality

$$\left|\sum_{k=1}^{N_{max}}Y_f(k)Y_g(k)\right|\le\left(\sum_{k=1}^{N_{max}}[Y_f(k)]^2\right)^{1/2}\left(\sum_{k=1}^{N_{max}}[Y_g(k)]^2\right)^{1/2} \tag{A10}$$

and we find

$$(F_f-F_g)^2\le F^2_{f+g}\le(F_f+F_g)^2\Rightarrow|F_f-F_g|\le F_{f+g}\le F_f+F_g. \tag{A11}$$

From Eqs. (A3) for $m=0$, in every box we have $\sum_{k=1}^n y(k)=\sum_{k=1}^n y_n(k)$. Thus we obtain $\sum_{k=1}^{N_{max}}Y_f(k)=\sum_{k=1}^{N_{max}}Y_g(k)=0$, where $Y_f(k)$ and $Y_g(k)$ fluctuate around zero. When $Y_f(k)$ and $Y_g(k)$ are not correlated, the value of
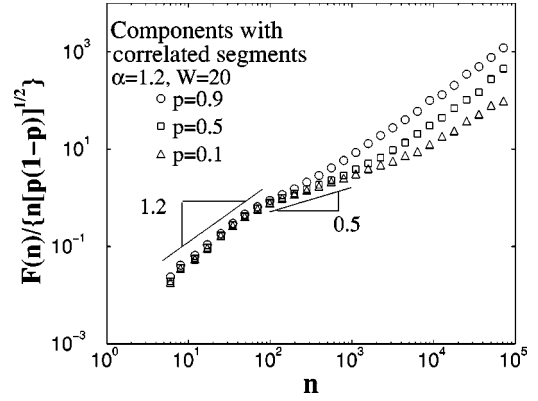

FIG. 10. Dependence of the scaling behavior of components on the fraction p of the segments with strong positive correlations ($\alpha=1.2$). The segment size is $W=20$ and the length of the components is $N_{max}=2^{20}$. After rescaling $F(n)/n$ by $\sqrt{p(1-p)}$, all curves collapse at small scales ($n<W$) with slope 1.2 and at intermediate scales with slope 0.5. The intermediate scale regime shrinks when p increases.

the third term in Eq. (A9) is close to zero and we obtain the following superposition rule:

$$F^2_{f+g}=F^2_f+F^2_g. \tag{A12}$$

APPENDIX B: STRONGLY CORRELATED SEGMENTS

For components containing segments with stronger positive correlations ($\alpha>1$) and fixed $W=20$, we find that at small scales ($n<W$), the slope of $F(n)/n$ does not depend on the fraction p and is close to that expected for a stationary signal $u(i)$ with identical correlations (Fig. 10). Surprisingly we find that in order to collapse the $F(n)/n$ curves obtained for different values of the fraction p, we need to rescale $F(n)/n$ by $\sqrt{p(1-p)}$ instead of $\sqrt{p}$, which is the rescaling factor at small scales for components containing segments with correlations $\alpha<1$. Thus $\alpha=1$ is a threshold indicating when the rescaling factor changes. Our simulations show that this threshold increases when the segment size W increases.

For components containing a sufficiently small fraction p of correlated segments ($\alpha>0.5$), we find that in the intermediate scale regime there is a crossover to random behavior with slope 0.5. The $F(n)/n$ curves obtained for different values of p collapse in the intermediate scale regime if we rescale $F(n)/n$ by $\sqrt{p(1-p)}$ (Fig. 10). We note that this random behavior regime at intermediate scales shrinks with the increasing fraction p of correlated segments and, as expected, for p close to 1 this regime disappears (see the $p=0.9$ curve in Fig. 10).

[1] R. L. Stratonovich, *Topics in the Theory of Random Noise* (Gordon and Breach, New York, 1981), Vol. 1.

[2] A. Witt, J. Kurths, and A. Pikovsky, Phys. Rev. E **58**, 1800 (1998).

[3] C.-K. Peng, S. V. Buldyrev, S. Havlin, M. Simons, H. E. Stan-

ley, and A. L. Goldberger, Phys. Rev. E **49**, 1685 (1994).

[4] M. S. Taqqu, V. Teverovsky, and W. Willinger, Fractals **3**, 785 (1995).

[5] C.-K. Peng, S. V. Buldyrev, A. L. Goldberger, S. Havlin, F. Sciortino, M. Simons, and H. E. Stanley, Nature (London) **356**,

168 (1992).

[6] C.-K. Peng, S. V. Buldyrev, A. L. Goldberger, S. Havlin, M. Simons, and H. E. Stanley, Phys. Rev. E **47**, 3730 (1993).

[7] S. V. Buldyrev, A. L. Goldberger, S. Havlin, C.-K. Peng, H. E. Stanley, and M. Simons, Biophys. J. **65**, 2673 (1993).

[8] S. M. Ossadnik, S. B. Buldyrev, A. L. Goldberger, S. Havlin, R. N. Mantegna, C.-K. Peng, M. Simons, and H. E. Stanley, Biophys. J. **67**, 64 (1994).

[9] H. E. Stanley, S. V. Buldyrev, A. L. Goldberger, S. Havlin, R. N. Mantegna, C.-K. Peng, and M. Simons, Nuovo Cimento D **16**, 1339 (1994).

[10] R. N. Mantegna, S. V. Buldyrev, A. L. Goldberger, S. Havlin, C.-K. Peng, M. Simons, and H. E. Stanley, Phys. Rev. Lett. **73**, 3169 (1994).

[11] S. Havlin, S. V. Buldyrev, A. L. Goldberger, S. M. Ossadniksm, C.-K. Peng, M. Simons, and H. E. Stanley, Chaos, Solitons Fractals **6**, 171 (1995).

[12] C.-K. Peng, S. V. Buldyrev, A. L. Goldberger, S. Havlin, R. N. Mantegna, M. Simons, and H. E. Stanley, Physica A **221**, 180 (1995).

[13] S. Havlin, S. V. Buldyrev, A. L. Goldberger, R. N. Mantegna, C.-K. Peng, M. Simons, and H. E. Stanley, Fractals **3**, 269 (1995).

[14] R. N. Mantegna, S. V. Buldyrev, A. L. Goldberger, S. Havlin, C.-K. Peng, M. Simons, and H. E. Stanley, Phys. Rev. Lett. **76**, 1979 (1996).

[15] S. V. Buldyrev, N. V. Dokholyan, A. L. Goldberger, S. Havlin, C.-K. Peng, H. E. Stanley, and G. M. Viswanathan, Physica A **249**, 430 (1998).

[16] H. E. Stanley, S. V. Buldyrev, A. L. Goldberger, S. Havlin, C.-K. Peng, and M. Simons, Physica A **273**, 1 (1999).

[17] C.-K. Peng, S. Havlin, H. E. Stanley, and A. L. Goldberger, Chaos **5**, 82 (1995).

[18] N. Iyengar, C.-K. Peng, R. Morin, A. L. Goldberger, and L. A. Lipsitz, Am. J. Physiol. **40**, R1078 (1996).

[19] P. Ch. Ivanov, M. G. Rosenblum, C.-K. Peng, J. E. Mietus, S. Havlin, H. E. Stanley, and A. L. Goldberger, Nature (London) **383**, 323 (1996).

[20] K. K. L. Ho, G. B. Moody, C.-K. Peng, J. E. Mietus, M. G. Larson, D. Levy, and A. L. Goldberger, Circulation **96**, 842 (1997).

[21] P. Ch. Ivanov, M. G. Rosenblum, C.-K. Peng, J. E. Mietus, S. Havlin, H. E. Stanley, and A. L. Goldberger, Physica A **249**, 587 (1998).

[22] M. Barbi, S. Chillemi, A. Di Garbo, R. Balocchi, C. Carpeggiani, M. Emdin, C. Michelassi, and E. Santarcangelo, Chaos, Solitons Fractals **9**, 507 (1998).

[23] P. Ch. Ivanov, A. Bunde, L. A. Nunes Amaral, S. Havlin, J. Fritsch-Yelle, R. M. Baevsky, H. E. Stanley, and A. L. Goldberger, Europhys. Lett. **48**, 594 (1999).

[24] S. M. Pikkujamsa, T. H. Makikallio, L. B. Sourander, I. J. Raiha, P. Puukka, J. Skytta, C.-K. Peng, A. L. Goldberger, and H. V. Huikuri, Circulation **100**, 393 (1999).

[25] P. Ch. Ivanov, L. A. Nunes Amaral, A. L. Goldberger, S. Havlin, M. G. Rosenblum, Z. R. Struzik, and H. E. Stanley, Nature (London) **399**, 461 (1999).

[26] S. Havlin, S. V. Buldyrev, A. Bunde, A. L. Goldberger, P. Ch. Ivanov, C.-K. Peng, and H. E. Stanley, Physica A **273**, 46 (1999).

[27] H. E. Stanley, L. A. Nunes Amaral, A. L. Goldberger, S. Havlin, P. Ch. Ivanov, and C.-K. Peng, Physica A **270**, 309 (1999).

[28] Y. Ashkenazy, M. Lewkowicz, J. Levitan, S. Havlin, K. Saermark, H. Moelgaard, and P. E. B. Thomsen, Fractals **7**, 85 (1999).

[29] T. H. Makikallio, J. Koistinen, L. Jordaens, M. P. Tulppo, N. Wood, B. Golosarsky, C.-K. Peng, A. L. Goldberger, and H. V. Huikuri, Am. J. Cardiol. **83**, 880 (1999).

[30] P. A. Absil, R. Sepulchre, A. Bilge, and P. Gerard, Physica A **272**, 235 (1999).

[31] S. Havlin, L. A. Nunes Amaral, A. L. Goldberger, P. Ch. Ivanov, C.-K. Peng, and H. E. Stanley, Physica A **274**, 99 (1999).

[32] D. Toweill, K. Sonnenthal, B. Kimberly, S. Lai, and B. Goldstein, Crit. Care Med. **28**, 2051 (2000).

[33] A. Bunde, S. Havlin, J. W. Kantelhardt, T. Penzel, J. H. Peter, and K. Voigt, Phys. Rev. Lett. **85**, 3736 (2000).

[34] T. T. Laitio, H. V. Huikuri, E. S. H. Kentala, T. H. Makikallio, J. R. Jalonen, H. Helenius, K. Sariola-Heinonen, S. Yli-Mayry, and H. Scheinin, Anesthesiology **93**, 69 (2000).

[35] Y. Ashkenazy, P. Ch. Ivanov, S. Havlin, C.-K. Peng, Y. Yamamoto, A. L. Goldberger, and H. E. Stanley, Comput. Cardiol. **27**, 139 (2000).

[36] Y. Ashkenazy, P. Ch. Ivanov, S. Havlin, C.-K. Peng, A. L. Goldberger, and H. E. Stanley, Phys. Rev. Lett. **86**, 1900 (2001).

[37] P. Ch. Ivanov, L. A. Nunes Amaral, A. L. Goldberger, M. G. Rosenblum, H. E. Stanley, and Z. R. Struzik, Chaos **11**, 641 (2001).

[38] J. M. Hausdorff, C.-K. Peng, Z. Ladin, J. Wei, and A. L. Goldberger, J. Appl. Physiol. **78**, 349 (1995).

[39] K. Ivanova and M. Ausloos, Physica A **274**, 349 (1999).

[40] E. Koscielny-Bunde, A. Bunde, S. Havlin, H. E. Roman, Y. Goldreich, and H. J. Schellnhuber, Phys. Rev. Lett. **81**, 729 (1998).

[41] E. Koscielny-Bunde, H. E. Roman, A. Bunde, S. Havlin, and H. J. Schellnhuber, Philos. Mag. B **77**, 1331 (1998).

[42] P. Talkner and R. O. Weber, Phys. Rev. E **62**, 150 (2000).

[43] A. Montanari, R. Rosso, and M. S. Taqqu, Water Resour. Res. **36**, 1249 (2000).

[44] C. Matsoukas, S. Islam, and I. Rodriguez-Iturbe, J. Geophys. Res., [Atmos.] **105**, 29 165 (2000).

[45] S. Bahar, J. W. Kantelhardt, A. Neiman, H. H. A. Rego, D. F. Russell, L. Wilkens, A. Bunde, and F. Moss, Europhys. Lett. **56**, 454 (2001).

[46] Y. Liu, P. Cizeau, M. Meyer, C.-K. Peng, and H. E. Stanley, Physica A **245**, 437 (1997).

[47] N. Vandewalle and M. Ausloos, Physica A **246**, 454 (1997).

[48] N. Vandewalle and M. Ausloos, Phys. Rev. E **58**, 6832 (1998).

[49] Y. Liu, P. Gopikrishnan, P. Cizeau, M. Meyer, C.-K. Peng, and H. E. Stanley, Phys. Rev. E **60**, 1390 (1999).

[50] I. M. Janosi, B. Janecsko, and I. Kondor, Physica A **269**, 111 (1999).

[51] M. Ausloos, N. Vandewalle, P. Boveroux, A. Minguet, and K. Ivanova, Physica A **274**, 229 (1999).

[52] M. Roberto, E. Scalas, G. Cuniberti, and M. Riani, Physica A **269**, 148 (1999).

[53] N. Vandewalle, M. Ausloos, and P. Boveroux, Physica A **269**, 170 (1999).

[54] P. Grau-Carles, Physica A **287**, 396 (2000).

[55] M. Ausloos, Physica A **285**, 48 (2000).

[56] M. Ausloos and K. Ivanova, Physica A **286**, 353 (2000).

[57] M. Ausloos and K. Ivanova, Phys. Rev. E **63**, 047201 (2001).

[58] M. Ausloos and K. Ivanova, Int. J. Mod. Phys. C **12**, 169 (2001).

[59] P. Ch. Ivanov, L. A. Nunes Amaral, A. L. Goldberger, and H. E. Stanley, Europhys. Lett. **43**, 363 (1998).

[60] J. W. Kantelhardt, E. Koscielny-Bunde, H. H. A. Rego, S. Havlin, and A. Bunde, Physica A **294**, 441 (2001).

[61] K. Hu, P. Ch. Ivanov, Z. Chen, P. Carpena, and H. E. Stanley, Phys. Rev. E **64**, 011114 (2001).

[62] M. A. Carskadon and W. C. Dement, *Principle and Practice of Sleep Medicine* (Saunders, Philadelphia, 2000).

[63] H. A. Makse, S. Havlin, M. Schwartz, and H. E. Stanley, Phys. Rev. E **53**, 5445 (1996).

[64] When $0 < \gamma < 1$, α, and γ have the following relation: $\alpha = (2 - \gamma)/2$.

[65] We note that for components containing strongly correlated segments (e.g., $\alpha = 1.2$ when $W = 20$, see Appendix B and Fig. 10), at small scales the contribution of the correlated nonzero segments $[F_{\text{corr}}(n)/n]$ is still substantial, however, we have $F(n)/n \approx F_{\text{corr}}(n)/n \sim A\sqrt{p(1-p)}n^{\alpha}$.